Mon. Not. R. Astron. Soc. **308,** 599–608 (1999)

Hot gas in clusters of galaxies: the punctuated equilibria model

A. Cavaliere,[1]⋆ N. Menci[2] and P. Tozzi[1]†
[1]*Astrofisica, Dipartimento Fisica, II Università di Roma, via Ricerca Scientifica 1, 00133 Roma, Italy*
[2]*Osservatorio Astronomico di Roma, via Osservatorio, 00040 Monteporzio, Italy*

Accepted 1999 January 29. Received 1998 November 28; in original form 1998 June 22

ABSTRACT

We develop our model of 'punctuated equilibria' for the hot intracluster gas emitting powerful X-rays. The model considers the gravitational potential wells set by the dark matter as they evolve by hierarchical clustering and engulf outer gas; it assumes that the gas readjusts to a new hydrostatic equilibrium after each merging event. Before merging the gas is heated at the virial temperature when bound in subclusters; at early z it is pre-heated by supernova activity following star formation.

In detail, we compute analytically the following steps: the dynamic histories of dark matter haloes with their merging events; the associated infall of gas into a halo, with compressions and shocks establishing the conditions at the cluster boundary; the updated disposition of the gas in the potential well, matching such conditions; and the statistical convolution of observable quantities over the merging histories.

For individual objects from groups to clusters, the model yields profiles of density and surface brightness with no free parameters; in particular, the so-called β parameter is itself an outcome of the model, and the polytropic index γ is internally constrained to a narrow range. We obtain mildly declining temperature profiles, and profiles for the density and for the surface brightness shallower in groups compared with clusters; our model groups also contain a lower baryonic fraction on average, but with a scatter considerably larger.

We present various key quantities over the whole range from groups to clusters. In particular, we predict in different cosmologies the statistical correlation L–T of X-ray luminosity with temperature; similarly, we derive the correlation R_X–T for the size of the X-ray emitting region. The intrinsic scatter in both correlations is also predicted.

Key words: methods: analytical – galaxies: clusters: general – intergalactic medium – X-rays: galaxies.

1 INTRODUCTION

Groups and clusters of galaxies constitute large, nearly virialized condensations. Within their virial radii R, ranging from 1/2 to a few Mpc, the density contrasts attain or exceed $\delta\rho/\rho_u \sim 2\times10^2$ relative to the background, and the corresponding masses M range from some 10^{13} to 10^{15} $M_\odot$, mainly in dark matter (DM).

These structures contain a large baryonic fraction $f \simeq 0.1$ in the form of a hot intracluster plasma (ICP) at temperatures $kT \sim GM m_H/10R \sim 0.5$–$10$ keV (m_H is the proton mass) with particle densities up to $n \sim 10^{-3}$ cm^{-3}. The ICP emits by thin thermal bremsstrahlung X-ray luminosities $L \propto n^2 T^{1/2} R^3$ ranging from 10^{42} to 10^{45} erg s^{-1}.

Recent observations of individual objects resolved in energy and angle with the *ASCA* and the *SAX* satellites arguably indicate radial temperature profiles declining outwards (Markevitch, Sarazin & Henriksen 1997; Molendi, private communication; see also Hughes, Gorenstein & Fabricant 1988). In several cases the thermal structure is complicated by hot spots (Honda et al. 1997; Markevitch et al. 1998). As for the statistical aspects, a steep correlation close to the overall form $L \propto T^3$ is known to hold for local clusters, but with a substantial scatter (Edge & Stewart 1991; Mushotzky 1994). Recently the observations have sampled higher redshifts out to $z \sim 0.5$ (Tsuru et al. 1997; Mushotzky & Scharf 1997), finding little significant evolution. Low-temperature, local systems have also been sampled, finding there indications of a slope steeper yet (Ponman et al. 1996). For $kT > 5$ keV a flattening towards $L \propto T^2$ has been detected by Allen & Fabian (1998).

In the near future the *AXAF* mission will substantially improve the space-resolved spectroscopy of many individual clusters, and shortly after the mission *XMM* will greatly enlarge the statistics of the L–T correlation. Corresponding upgrades are called for in the theoretical understanding of the complex

⋆ E-mail: cavaliere@roma2.infn.it
†Present address: Department of Physics and Astronomy, The Johns Hopkins University, Baltimore, MD 21218, USA.

astrophysics concerning both the DM and the ICP over the full range from groups to clusters.

The force approach uses numerical computations for both the DM and the ICP, striving for wide dynamic range and complete hydrodynamics. The *N*-body simulations have shown, in accord with the hierarchical clustering picture (see Peebles 1993), the evolution of the DM haloes to occur largely through a sequence of merging and accretion events, which involve generally smaller partners down to nearly diffuse matter (see, e.g., Tormen, Bouchet & White 1997), and are correlated with the surrounding large-scale structures (Colberg et al. 1997).

As for the ICP, pioneering work by Schindler & Müller (1993) taken up by Roettiger, Stone & Mushotzky (1998) used 3D Eulerian codes with adaptive mesh and advanced shock-capturing methods to study how the large merging events of the DM haloes affect the ICP component. The outcomes show how such events produce anisotropic shocks and non-uniform compressions, resulting in a complex thermal structure lasting a few gigayears.

At the other extreme, a sequence of radial, highly resolved Eulerian computations (progressing from Perrenod 1980 to Takizawa & Mineshige 1998a) have shown that isotropic accretion of smooth gas also causes a strong and slowly expanding shock, which remains close to the (growing) virial radius for some dynamical times.

Most recently, state-of-the-art *N*-body codes coupled with advanced hydrodynamics (Bryan & Norman 1998; Gheller, Pantano & Moscardini 1998) have been run on supercomputers, aiming at resolutions below 100 kpc in rich clusters as necessary for deriving reliable luminosities. But such simulations are hard-pressed in implementing at the same time the full physics of the ICP. In fact, pre-heating at temperatures $\sim$0.5 keV is expected from stellar formation and evolution to supernovae (see Renzini 1997, and references therein); this is particularly relevant for the shallower potentials of groups where T is close to 0.5 keV. Inclusion of the pre-heating in the numerical work is technically taxing, as it involves cooling, star formation and energy feedback resolved down to subgalactic scales; but in its absence the simulations produce a correlation of the form $L \propto T^2$ at all temperatures, at variance with the data. Suginohara & Ostriker (1998) stress how delicate the balance of cooling and feedbacks may become at high resolutions, and how difficult it is to reproduce ICP cores as observed. Thus for now and for some time to come it will be hard to combine into a realistic numerical picture the wide dynamic range from galaxies to large-scale structures, stellar pre-heating and large statistics.

The state of the numerical approach and the challenge from the data motivates us to present here an *analytic* model that includes, though in a simplified form, the physical processes outlined above. We describe the cluster history as a sequence of *punctuated equilibria* (PE). That is to say, we envisage such history as a sequence of hierarchical merging episodes of the DM haloes, which we compute analytically (with its variance) in the framework of the standard hierarchical clustering, specifically using the so-called 'extended Press and Schechter theory' (Bond et al. 1991; Bower 1991; Lacey & Cole 1993). We stress that such episodes cause in the gas shocks of various strengths depending on the mass ratio of the merging subclusters, ranging from nearly adiabatic compressions for comparable clumps up to shocks with high Mach numbers in the accretion of loose gas. Our point is that the most effective of such shocks and compressions overlap to provide the boundary conditions for the new hydrostatic equilibrium to which the ICP is assumed to readjust.

The PE model as presented here takes up our previous work (Cavaliere, Menci & Tozzi 1997, 1998, hereafter CMT97, CMT98), but differs in that the histories of the DM haloes are now computed *analytically* rather than based on Monte Carlo simulations. This goes beyond the technical aspect since it allows us to explore efficiently the dependences of the density, temperature and luminosity on the parameters of the clusters and on the cosmology. In the same vein, the present approach allows us to quantify the connection between slope and scatter of the L–T correlation and the cosmological scenario. In addition, the parameters of the ICP thermal state are now fixed or bounded in terms of constraints internal to the model, and *new* predictions are presented.

In Section 2 we describe the PE model and our computational steps: in Section 2.1 we recall the statistical formalism for hierarchically merging DM haloes; in Section 2.2, we derive from the mass ratios involved in each merging episode the boundary conditions for the plasma equilibrium; in Section 2.3 we compute from such boundary conditions the ICP equilibrium; in Section 2.4 we derive the statistics of L and of the size R_X using the formalism of Section 2.1. In Section 3 we give, and compare with the observations, the model results for the profiles $n(r)$ and $T(r)$, for the surface brightness $\Sigma(r)$, for the relations M–T and f–T, and for the correlations R_X–T and L–T. The final Section 4 is devoted to discussion and conclusions.

2 THE PUNCTUATED EQUILIBRIA MODEL

The continuum X-ray bolometric luminosity of a cluster is given in its basic dependences by

$$L \propto \int_0^{r_2} n^2(r)\, T^{1/2}(r)\, \mathrm{d}^3 r. \tag{1}$$

Here $T(r)$ is temperature in the plasma and r_2 is the cluster boundary, which we take to be close to the virial radius $R \propto M^{1/3}\, \rho^{-1/3}$, where $\rho(z) \propto (1+z)^3$ is the DM density in the cluster, proportional to the average cosmic DM density $\rho_u(z)$ at formation.

It will be convenient to separate the internal profiles $n(r)$ and $T(r)$ from their boundary conditions at r_2. As to the latter, the infalling gas is expected to become supersonic near r_2 (see, e.g., Perrenod 1980; Takizawa & Mineshige 1998a) so that a shock front will form there. The conservations of mass, energy and stresses across the shock yield the Rankine–Hugoniot conditions, i.e., the temperature and density jumps from the outer values T_1 and n_1 to T_2 and n_2 just interior to r_2 (spelled out in Section 2.2). Then the luminosity may be rewritten in the form

$$L \propto r_2^3\, n_2^2\, T_2^{1/2} \int_0^1 \mathrm{d}^3 x \left[\frac{n(x)}{n_2}\right]^2 \left[\frac{T(x)}{T_2}\right]^{1/2}, \tag{2}$$

where $x \equiv r/r_2$.

Note that the values n_2 and T_2 at the boundary are not uniquely determined by the cluster mass M; rather, they are related to the outer values n_1 and T_1 by the named shock conditions. In turn, n_1 is fixed by $n_1 \propto f_u\, \rho_u / m_H$, in terms of the universal baryonic fraction f_u; whereas T_1 is determined only statistically, through the diverse merging histories ending up in the mass M. Specifically, as explained in detail in Sections 2.1 and 2.2, in each merging episode T_1 takes on the values appropriate to the other merging partner, constituted by lumps or even by smooth gas. In sum, a given dark mass M admits a set of ICP equilibrium states characterized by different boundary conditions, each corresponding to a different realization of the dynamical merging history. It is the convolution over such a set that provides the average values of L and R_X, and their scatter.

So the development of our PE model proceeds along the following steps:

(i) we first give the statistics of the current DM halo of mass M and of the merging clumps ΔM;

(ii) we compute the shock strength relating at the boundary the inner values T_2 and n_2 to the exterior ones T_1 and n_1, as a function of M and ΔM;

(iii) from such boundary values, we compute the internal profiles $T(x)/T_2$ and $n(x)/n_2$ for the post-merging hydrostatic equilibrium, involving the cluster potential and hence M; and

(iv) we convolve the results of steps (ii) and (iii) with the statistics (i).

Below we describe these steps in turn.

2.1 Histories of the dark matter haloes

Here we recall the basic merging probabilities provided by the 'extended Press & Schechter theory' (see Lacey & Cole 1993, 1994). This is based on the dark haloes formed by hierarchical merging of smaller structures.

The halo mass distribution at the cosmic time t is given by the standard Press & Schechter (1974) formula

$$N(m,t) = \sqrt{\frac{2}{\pi}}\,\frac{\delta_{\rm c}(t)\,\rho_{\rm u}}{M_0^2}\,\left|\frac{{\rm d}\ln\sigma}{{\rm d}\ln m}\right|\,\frac{m^{-2}}{\sigma(m)}\,{\rm e}^{-\frac{\delta_{\rm c}(t)^2}{2\,\sigma^2(m)}}, \qquad (3)$$

where the masses $m \equiv M/M_0$ are normalized to the current value $M_0 = 0.6\times10^{15}\,\Omega_0\,h^{-1}{\rm M}_\odot$ (i.e., to the mass enclosed within a sphere of radius $8\,h^{-1}$ Mpc), and $\delta_{\rm c}(t) = \delta_{\rm co}\,D(t)$ is a critical threshold for the collapse and virialization of the primordial density perturbations. The local value $\delta_{\rm co}$ depends weakly on the cosmological parameters, while the growth factor $D(t)$ depends sensitively on them. The mass variance $\sigma(m)$ is computed in terms of the perturbation spectrum; for definiteness, we use the cold dark matter (CDM) spectra given and discussed by White et al. (1996). For $\Omega = 1$ we adopt the primordial 'tilted' index $n_{\rm p} = 0.8$; for $\Omega_0 < 1$ we adopt $n_{\rm p} = 1$. The associated normalizations are taken from the *COBE*/DMR data (Gorski et al. 1998), and expressed in terms of the amplitude σ_8 at the relevant scale of $8\,h^{-1}$ Mpc (see Bunn & White 1997).

Corresponding to equation (3), the probability distribution that a given mass m at time t_0 has a progenitor of mass m' at time $t_1 < t_0$ reads

$$\frac{{\rm d}f}{{\rm d}m'}(m',t_1|m,t_0) = \frac{\delta_{\rm c}(t_1)-\delta_{\rm co}}{(2\pi)^{1/2}(\sigma'^2-\sigma^2)^{3/2}}\,\frac{m}{m'}\,\left|\frac{{\rm d}\sigma'^2}{{\rm d}m'}\right| \times\exp\left\{-\frac{[\delta_{\rm c}(t_1)-\delta_{\rm co}]^2}{2\,(\sigma'^2-\sigma^2)}\right\}, \qquad (4)$$

where σ' is the mass variance at the scale m'. On the other hand, at a given time t a progenitor m' increases its mass by a merging event with a clump of mass Δm (producing a cluster with mass $m = m' + \Delta m$), with the probability distribution per unit time given by

$$\frac{{\rm d}^2p(m'\rightarrow m'+\Delta m)}{{\rm d}\Delta m\,{\rm d}t} = \left(\frac{2}{\pi}\right)^{1/2}\left|\frac{{\rm d}\,\ln(\delta_{\rm c})}{{\rm d}t}\right|\left|\frac{{\rm d}\,\ln\sigma}{{\rm d}m}(m'+\Delta m)\right| \times\frac{\delta_{\rm c}(t)}{\sigma(m'+\Delta m)} \times\frac{1}{\left[1-\sigma^2(m'+\Delta m)/\sigma^2(m')\right]^{3/2}} \times\exp\left\{-\frac{\delta_{\rm c}^2(t)}{2}\left[\frac{1}{\sigma^2(m'+\Delta m)}-\frac{1}{\sigma^2(m')}\right]\right\}. \qquad (5)$$

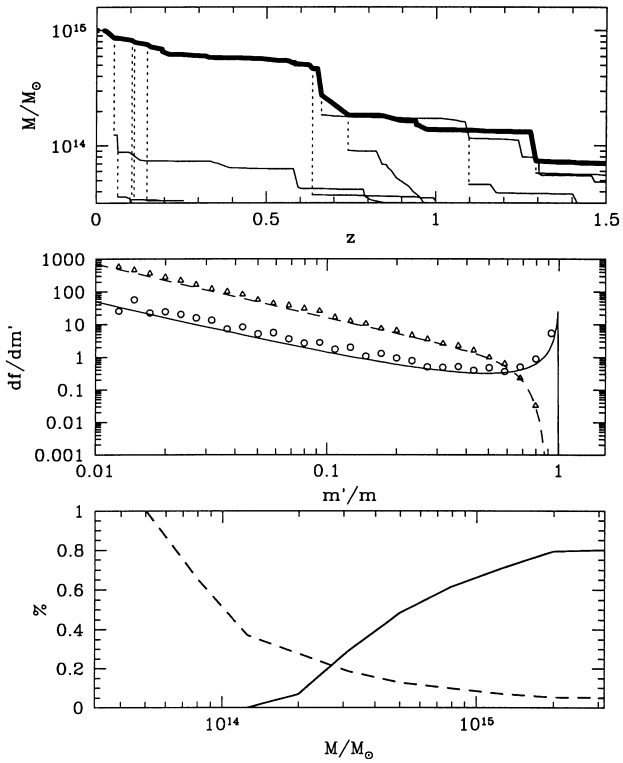

Figure 1. *Top panel*: A Monte Carlo realization to illustrate the merging history of a DM halo with final mass $10^{15}\,{\rm M}_\odot$. *Middle panel*: For the same halo, the probability distribution of progenitors with mass M' at the redshifts $z = 0.03$ and 0.5 that end up in a mass M at $z = 0$. The circles ($z = 0.03$) and the triangles ($z = 0.5$) represent the results from the Monte Carlo simulations, while the lines show the analytical results from equation (4). *Bottom panel*: The fraction of merging events during the last 2 Gyr involving a mass M and a partner with mass $3\times10^{13}\,{\rm M}_\odot < M' < M/10$ (solid line); the lower limit arises from requiring a virial temperature $T_{\rm v} > 0.5$ keV for the partner (see Section 2.2). The dashed line is the corresponding fraction for events with $M' > M/2.5$. We adopt a tilted, *COBE*-normalized spectrum of perturbations, as given in White et al. (1996) in the critical universe with $H_0 = 50$ km s^{-1} Mpc^{-1}.

We have compared the analytical probabilities above with the results of the Monte Carlo code developed by P. Tozzi to simulate the hierarchical merging history of haloes, based on the excursion set approach of Bond et al. (1991). A realization from the Monte Carlo simulations is shown in Fig. 1 (top) as an illustration of the basic process of DM halo growth. To show the agreement of the two approaches for a relevant quantity, we also plot in Fig. 1 (middle) the probability distribution of progenitors of mass m' at different z that end up in a given mass m at $z = 0$, computed from the Monte Carlo and from the equations above. In the bottom panel of Fig. 1 we show as a function of m the fraction of objects which, during the last 2 Gyr, accreted mass in events involving comparable clumps (specifically, those with mass ratio 1/2.5), and in events involving very unequal clumps (with mass ratio 1/10); during that interval, more than 60 per cent of the clusters with $M \geq 10^{15}\,{\rm M}_\odot$ will have merged with clumps smaller than $M/10$.

2.2 Boundary conditions

The pre-shock temperature in a merging event is that of the infalling gas. If the latter is contained in a sufficiently deep potential well, T_1 is the virial temperature $T_{1{\rm v}} \propto \Delta m/r$ of the secondary merging

partner; on using $r \propto (\Delta m/\rho)^{1/3}$ this can be written

$$k\,T_{1\mathrm{v}} = 4.5\,(\Delta m)^{2/3}\,(\rho/\rho_0)^{1/3}\ \mathrm{keV}, \tag{6}$$

where the numerical coefficient is taken from Hjorth, Oukbir & van Kampen (1998). Where necessary, the z dependence of $\rho/\rho_0 = (1+z)^3$ is converted to t dependence following the standard FRW cosmologies.

But an independent lower bound $kT_{1*} \approx 0.5$ keV is provided by pre-heating of diffuse external gas, because of feedback energy inputs following star formation and evolution all the way to supernovae (David, Jones & Forman 1995; Renzini 1997). We recall that pre-heating temperatures in excess of 0.1 keV are believed to constitute essential complements to the hierarchical clustering picture to prevent the 'cooling catastrophe' from occurring (see White & Rees 1978; Blanchard, Valls-Gabaud & Mamon 1992). In point of fact, Henriksen & White (1996) find from X-rays evidence for diffuse gas at 0.5–1 keV in the outer regions of a number of clusters. So in the following the actual value of T_1 will be

$$T_1 = \max\,\left[T_{1\mathrm{v}}, T_{1*}\right]. \tag{7}$$

Given T_1, the boundary conditions for the ICP in the cluster are set by the strength of the shocks separating the inner from the infalling gas. We report here from CMT98 the explicit expression of the post-shock temperature T_2 for three degrees of freedom and for a nearly hydrostatic post-shock condition with $v_2 << v_1$, assuming the shock velocity to match the growth rate of the virial radius $R(t)$:

$$kT_2 = \frac{\mu m_{\mathrm{H}} v_1^2}{3}\left[\frac{(1+\sqrt{1+\epsilon})^2}{4} + \frac{7}{10}\epsilon - \frac{3}{20}\frac{\epsilon^2}{(1+\sqrt{1+\epsilon})^2}\right]. \tag{8}$$

Here $\epsilon \equiv 15kT_1/4\mu m_{\mathrm{H}} v_1^2$ and μ is the average molecular weight; the inflow velocity v_1 is set by the potential drop across the region of nearly free fall, to read $v_1 \simeq \sqrt{-\phi_2/m_{\mathrm{H}}}$ in terms of the potential ϕ_2 at r_2. For a 'cold inflow' with $\epsilon << 1$ the shock is *strong*, and the expression simplifies to $kT_2 \simeq \mu m_{\mathrm{H}} v_1^2/3 + 3kT_1/2$. In contrast, for $\epsilon \gtrsim 1$ the shock is *weak*, and $T_2 \simeq T_1$ is recovered as expected. Note that T_2 depends through both T_1 and v_1^2 on the mass Δm of the clump being accreted.

From T_2 and T_1, the density jump at the boundary n_2/n_1 is found to read (see CMT97)

$$\frac{n_2}{n_1} = 2\left(1 - \frac{T_1}{T_2}\right) + \left[4\left(1 - \frac{T_1}{T_2}\right)^2 + \frac{T_1}{T_2}\right]^{1/2}. \tag{9}$$

It is seen that the density jump takes on the limiting value $n_2/n_1 = 4$ for very strong shocks, while the adiabatic approximation $n_2/n_1 \approx 1 + 3(T_2 - T_1)/2T_1$ is recovered for weak shocks.

2.3 Hydrostatic equilibrium

We adopt the polytropic temperature description $T(x)/T_2 = [n(x)/n_2]^{\gamma-1}$, with the index γ in the range $1 \le \gamma \le 5/3$ to begin with. In terms of the virial temperature T_{v} (see Sarazin 1988), equation (2) can be written

$$L \propto r_2^3\,(n_1/\rho)^2\,(n_2/n_1)^2\,T_{\mathrm{v}}^{1/2}\,\rho^2\left(T_2/T_{\mathrm{v}}\right)^{1/2}\,\overline{\left[n(r)/n_2\right]^{2+(\gamma-1)/2}},$$

where the bar denotes the integration over the emitting volume $r^3 \le r_2^3$, and ρ is the average DM density in the cluster, proportional to ρ_{u} and so to n_1 (see equation 2). The radius r_2 may be rewritten in terms of the temperature $T_{\mathrm{v}} \propto m/r_2 \propto \rho\, r_2^2$. We finally obtain

$$L \propto \left(\frac{n_2}{n_1}\right)^2 T_{\mathrm{v}}^2\,\rho^{1/2}\left[\frac{T_2}{T_{\mathrm{v}}}\right]^{1/2}\overline{\left[n(r)/n_2\right]^{2+(\gamma-1)/2}}. \tag{10}$$

The underlying assumption is that after a merging event the cluster readjusts to a hydrostatic equilibrium with boundary conditions n_2, T_2 corresponding to its dynamical history (see equation 6–9). Actually, this requires sound propagation times shorter than the dynamical time-scale taken anyway by the DM to relax to its own steady configuration; the assumption is seen to be valid, though marginally, for all merging events except for the *rare* ones involving comparable clumps. As we discuss in detail in the concluding Section 4, the observations and the hydrodynamical N-body simulations concur in supporting not only the hydrostatic equilibrium approximation for the relevant merging events, but also its parametrization with a polytropic equation of state.

The ratio $n(x)/n_2$ is obtained from the hydrostatic equilibrium

$$\mathrm{d}P/m_{\mathrm{H}}\,n\,\mathrm{d}r = -GM(<r)/r^2 = -\mathrm{d}\phi/\mathrm{d}r$$

with the polytropic pressure

$$P(r) = kT_2\,n_2\left[n(r)/n_2\right]^{\gamma}.$$

This yields (see Cavaliere & Fusco Femiano 1978; Sarazin 1988, and references therein) the profiles

$$\frac{n(r)}{n_2} = \left[\frac{T(r)}{T_2}\right]^{1/(\gamma-1)} = \left\{1 + \frac{\gamma-1}{\gamma}\,\beta\left[\tilde{\phi}_2 - \tilde{\phi}(r)\right]\right\}^{1/(\gamma-1)}, \tag{11}$$

where $\tilde{\phi} \equiv \phi/\mu\, m_{\mathrm{H}}\,\sigma_2^2$ is the potential normalized to the associated one-dimensional DM velocity dispersion at r_2. The ICP disposition in equation (11) relative to the DM depends on the parameter

$$\beta = \mu m_{\mathrm{H}}\sigma_2/kT_2, \tag{12}$$

and is further modulated by the second parameter γ, to yield as the latter increases flatter profiles $n(r)$ and steeper $T(r)$. In our PE β is given by T_2 in equation (8), and considering the statistics of T_2 we obtain the results discussed in Section 3.1; the other parameter γ will be bounded as also discussed there.

We shall focus on the 'universal' forms of $\phi(r)$ and $\sigma(r)$ given by Navarro, Frenk & White (1997). When relevant, we will discuss also results for the (simplified) King potential (see Sarazin 1988; see also Adami et al. 1998) where the DM itself has a core, and somewhat fatter ICP cores obtain. We shall also discuss the steeper cusp found by Moore et al. (1997) in highly resolved CDM simulations; correspondingly, we still obtain a core-like ICP distribution, albeit slightly slimmer. Actually, in hydrostatic equilibrium a DM cusp flatter than $\rho(r) \propto r^{-2}$ (corresponding to a gravitational force flatter than r^{-1}) implies at the centre a finite ICP density n_{c} but a high derivative, which however at observable resolutions is flattened by a modest increase of γ.

2.4 Statistics

Our purpose is to compute the average value of L and its dispersion, associated with a given cluster mass m. We reiterate from Section 2 that the diverse merging histories ending up in such a mass give rise to a set of equilibrium states characterized by different values of T_2, n_2. These are related by equations (8) and (9) to the values of T_1 associated with the clump of mass Δm incoming on to a cluster progenitor. So to meet our purpose we must sum over the shocks produced at a time $t' < t$ in all possible progenitors m' (weighting with their number) by the accreted clumps Δm (weighting with their merging rate); finally, we integrate over times t' from an effective lower limit $t - \Delta t$.

The average L is then given by

$$\langle L\rangle = Q\int_{t-\Delta t}^{t}\mathrm{d}t'\int_0^m \mathrm{d}m'\int_0^{m-m'}\mathrm{d}\Delta m \times\frac{\mathrm{d}f}{\mathrm{d}m'}(m',t'|m,t)\,\frac{\mathrm{d}^2p(m'\rightarrow m'+\Delta m)}{\mathrm{d}\Delta m\,\mathrm{d}t'}\,L; \tag{13}$$

and the variance is given by

$$\langle \Delta L^2 \rangle = Q \int_{t-\Delta t}^{t} \mathrm{d}t' \int_0^m \mathrm{d}m' \int_0^{m-m'} \mathrm{d}\Delta m \times \frac{\mathrm{d}f}{\mathrm{d}m'}(m', t'|m, t) \frac{\mathrm{d}^2 p(m' \rightarrow m' + \Delta m)}{\mathrm{d}\Delta m \, \mathrm{d}t'} \Big(L - \langle L \rangle\Big)^2. \quad (14)$$

Higher moments – if needed in the case of non-Poissonian statistics – are given by similar expressions; the full distribution of L requires aimed computations or simulations, as noted by CMT98. In the integrals, the luminosity $L\left[T_2(m'), T_1(\Delta m')\right]$ depends on m' and $\Delta m'$ through the boundary conditions discussed in Section 2.2. The compounded probability distribution in equations (13) and (14) has been normalized to 1 (we do not write down the normalization factor Q for the sake of simplicity). The effective lower limit for the integration over masses is set as follows.

The merging events relevant to $\langle L \rangle$ and to $\langle \Delta L^2 \rangle$ after equations (13) and (14) are those lasting long enough so as to overlap with similar ones. Since $\Delta t \propto \Delta m / v_1 \, \rho \, r^2$, the above condition results in an effective lower limit for the masses entering equations (13) and (14); physically, lumps with masses smaller than such a limit yield a small mass flux and so produce shocks that dissipate before new clumps are incoming. We pinned down the minimum Δm numerically, by looking at the saturation of $\langle L \rangle$ for increasing values of Δt. This occurs at $\Delta t \approx 0.7 \, t_\mathrm{d}$, which corresponds to a lower limit about $m/20$ for Δm on using $r^2 \propto \Delta m^{2/3}$.

Note that the above procedure acts like an effective mass weight. Heuristically, this may be seen with the Δm and t integrations interchanged; then the lower limit contains $\Delta t(\Delta m)$, which must be convolved with the distribution of Δm. But for $\Delta t > 0.7 \, t_\mathrm{d}$ the resulting average saturates; so we have written the t integration as the outermost integral, having adopted the lower limit for Δm as said above.

Thus very small accreted lumps do not affect our average $\langle L \rangle$, owing to the small associated mass accretion rate. On the other hand, merging events involving comparable partners (though contributing $\sim$1/2 of the total mass) affect the overall $\langle L \rangle$ only marginally; in fact, such events not only are few (<10 per cent), but also involve lumps with temperatures T_1 comparable to T_2, and so produce a compression factor $n_2/n_1 \approx 1$ (equation 9). The major contribution to $\langle L \rangle$ is by far ($\sim$90 per cent) provided by intermediate merging lumps, which yield an *integrated* contribution $\sim$1/2 to the mass, but dominate the number of events and produce large compressions $(n_2/n_1)^2 \propto L$. For such events, the isotropic hydrostatic equilibrium for the ICP is physically motivated and robust (see Sections 2.3 and 4), substantiating our step-by-step treatment of the hydrodynamics.

3 RESULTS

Here we present various results from the PE model, and compare them with observations. To this aim, we shall express our results in terms of the observed emission weighted temperature, which we denote simply by T. Moreover, the contribution of relevant emission lines to L (from updates of Raymond & Smith 1977) has been added to the bremsstrahlung emission underlying the simple scaling in equation (10).

3.1 Profiles

Our reference cluster will have a mass m, and DM potential $\phi(r)$ as said in Section 2.3. The density and temperature profiles are given by equation (11), and are to match the shock boundary conditions at the position $r_2 \simeq R$. The key quantity is the parameter β defined by equation (12); its average value and scatter are *predicted* by the PE model [using convolutions analogous to equations (13) and (14)] to be as shown in Fig. 2. Note that $\beta(T)$ grows slowly with the temperature; we obtain values ranging from about $\beta = 0.5$ at the group scale to $\beta \approx 0.9$ for rich clusters (see Fig. 2). These values imply that in our model the ICP profiles are smoother and more extended than the DM profiles, an effect becoming more pronounced in scaling down from clusters to groups.

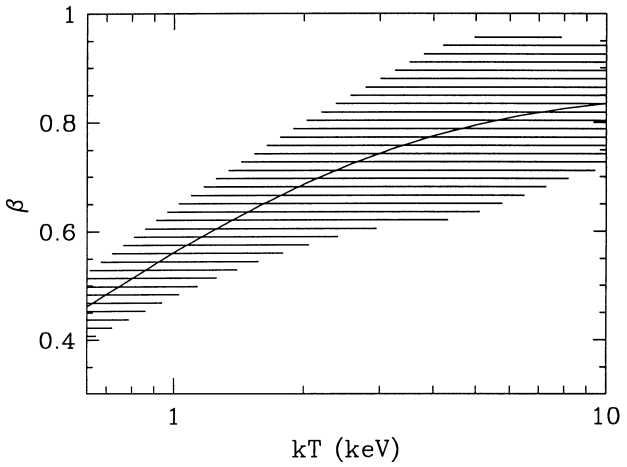

Figure 2. The predicted dependence of β on the (emission-weighted) temperature T (see equations 12 and 8). DM potential as given by Navarro et al. (1997), computed for the cosmological parameters and the perturbation power spectrum used in Fig. 1. The shaded region indicates the 2σ scatter resulting from the merging histories.

In Fig. 3 we show the baryonic fraction f_2 (integrated out to the shock) as a function of T and for different values of γ. The polytropic index $\gamma \geq 1$ describes the equation of state for the ICP. An upper bound to it arises if the overall thermal energy of the ICP is not to exceed its gravitational energy, with only minor contributions from other energy sources, like radio source heating or energy transfer from DM to ICP, as discussed in Section 4. The thermal and the gravitational energy are computed using the profiles in equation (11), and their ratio is given in Fig. 4 to show that the *upper* bound $\gamma \leq 1.3$ holds.

In Fig. 5 we show temperature profiles $T(r)$ for different values of γ, in terms of the normalized coordinate $x = r/R$. It turns out that the observations by Markevitch et al. (1997) are consistent with $T(r)$

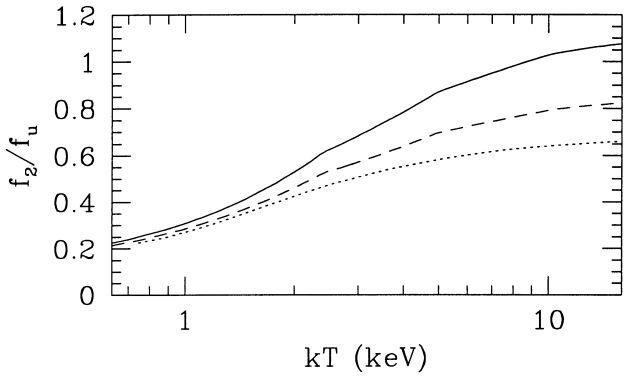

Figure 3. The predicted ratio of the baryonic fraction f_2 at the cluster boundary to the external value f_u (White et al. 1993; White & Fabian 1995) as a function of the temperature T for $\gamma = 1$ (solid line), $\gamma = 1.1$ (dashed) and $\gamma = 1.3$ (dotted).

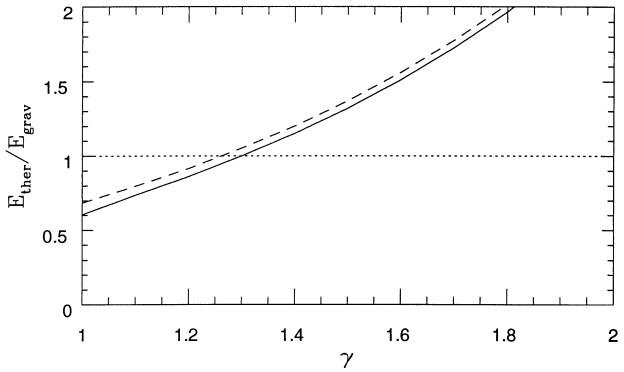

Figure 4. The ratio of the thermal ICP energy $E_{\rm ther} = 3\int {\rm d}^3 r\, n(r)\, T(r)$ to the ICP gravitational energy $E_{\rm grav} = G m_{\rm H} \int {\rm d}^3 r\, n(r)\, M(<r)/r$ as a function of γ for the DM potential of Fig. 2 (solid line), and for the King form (dashed line) with core radius $R/10$. The profiles $n(r)$ and $T(r)$ are provided by equation (11).

predicted when $\gamma = 1.2 \pm 0.1$, our allowed range. Hereafter we shall focus on $\gamma = 1.2$ for definiteness.

In Fig. 6 we show the density profiles $n(r)$ for two local clusters with different temperatures; the associated surface brightness $\Sigma(r)$ is shown in Fig. 7 along with representative data. It can be seen that groups have *flatter* $\Sigma(r)$ than rich clusters, an outcome persisting when the King or the Moore et al. (1997) potentials are used.

3.2 Correlations

We show first in Fig. 8 the M–T relation in view of its important role. Note that, given the mass function, our flattening at low temperatures translates into a steepening of the corresponding temperature function; such an effect has also been noted by Balogh, Babul & Patton (1998).

The local L–T correlation is given by the double convolution (13), and likewise for ΔL after equation (14). The results are shown in Fig. 9 for a tilted CDM spectrum of perturbations in the critical universe. For the reasons discussed in CMT98, the normalization has been best-fitted on the data.

As stressed in our previous works (CMT97; CMT98), the correlation we predict and show in Fig. 9 is *not* a single power law; it starts as $L \propto T^2$ for very rich clusters with high T, but bends down with decreasing T, owing to the threshold effect of the pre-heating temperature $kT_1 \approx 0.5$ keV. Note that our correction to 0.3 solar metallicity tends to increase, if anything, the luminosities and

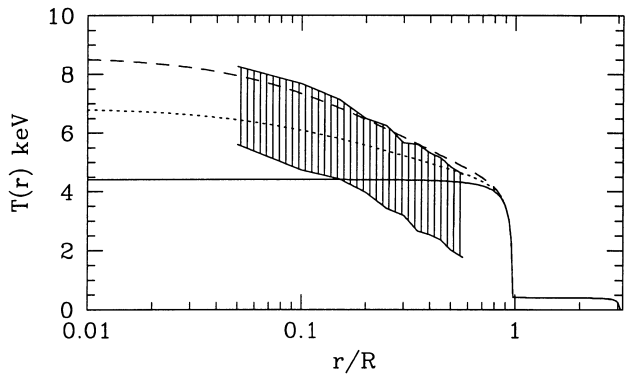

Figure 5. Temperature profiles for the model cluster of $10^{15}\,{\rm M}_\odot$ at $z = 0$ in polytropic equilibrium; $\gamma = 1$ (solid line), 1.2 (dotted) and 1.66 (dashed), see equation (11). DM potential as in Fig. 2. The profile is smoothed out with a filter width of 100 kpc. The dashed area taken from Markevitch et al. (1997) summarizes the observations of 30 clusters.

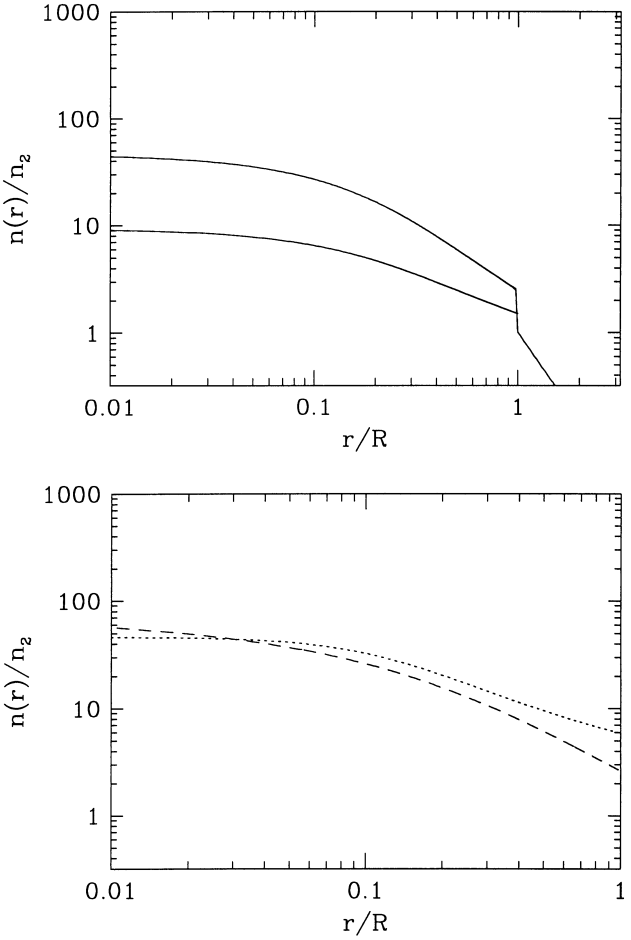

Figure 6. *Upper panel:* The predicted ICP density profile $n(r)$ for a rich cluster with $kT = 8$ keV (upper line), and for a poor cluster with $kT = 2$ keV (lower line). Radii are normalized to the virial radius R. The profiles are computed using the DM potential as in Fig. 2, and for the ICP the polytropic index $\gamma = 1.2$. *Bottom panel*: The variations produced by the use of the King potential as in Fig. 4, with $\gamma = 1.1$ (dotted line); and of the Moore et al. (1997) potential, with $\gamma = 1.3$ (dashed line).

to flatten the slope at low T.

A convenient fitting formula for the predicted L–T correlation (precise to better than 10 per cent for $T > 2\,T_1$) is as follows:

$$L = a_L\, T^{2+\alpha_L}\, (\rho/\rho_0)^{1/2},$$
$$a_L \propto 3.8\,\Omega_0^{0.3}\,(1+z)^{0.22/\Omega_0} + (1-\Omega_0)\,{\rm e}^{-0.7\,(1+z)}, \qquad (15)$$
$$\alpha_L = 1.12\,(1+z)^{-0.2}\,{\rm e}^{-0.25\,(T-T_1)/\Omega_0^{0.1}\,(1+z)^{0.5}},$$

where the luminosity is expressed in units of $10^{44}\,{\rm erg\,s^{-1}}$ and the temperature in keV. The z dependence of a_L results from the interplay of the following effects: (i) the evolution of the Navarro et al. (1997) potential; (ii) the abundance of clusters with given T; and (iii) the evolution of the progenitor probability distributions in equations (4) and (5). Such effects are small, and moreover they very nearly balance out, leaving the basic z dependence $[\rho(z)/\rho_0]^{1/2}$. In turn, the latter dependence goes as $(1+z)^{0.5-1}$, considering (CMT98) the evolution of the overdensities in the large-scale structures – filamentary or sheet-like – that are hosts to the clusters.

At temperatures substantially larger than the threshold $kT_1 \simeq 0.5$ keV, the intrinsic, dynamic dispersion grows with T, but the relative $\Delta L/L$ stays nearly constant around 25 per cent (2σ), as shown by Fig. 9. We have deliberately chosen to keep this

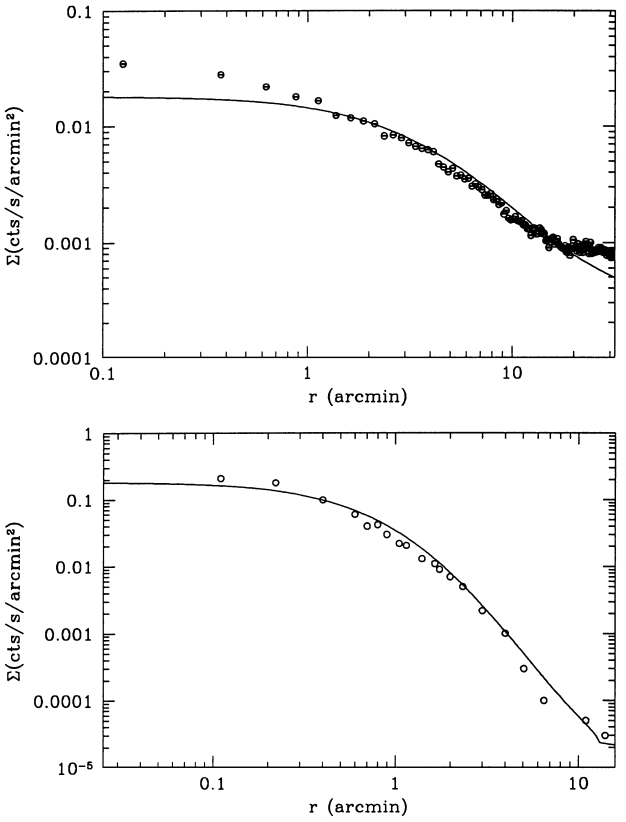

Figure 7. The surface brightness profile $\Sigma(r)$ from the PE model compared with the data for two oppositely extreme clusters. *Top panel*: A539, rather sparse and with low T, at $z = 0.026$ (David et al. 1996; De Simone, private communication). *Bottom panel*: A2390, relaxed and hot, at $z = 0.23$ (Böhringer et al. 1998). No attempt has been made to exclude emissions from cooling flows.

figure simple and not to include the conceivable spread of T_1 already represented by CMT98 in their Fig. 2; the effect of such a spread is to widen the dispersion below 1 keV, adding another, large component to the intrinsic dynamic variance.

As our analytical approach allows us to span a wide range of cosmologies/cosmogonies, we show in Fig. 10 (left) the dependence of $\langle L\rangle$ on Ω_0 at two temperatures and at the current epoch. It is seen that $\langle L\rangle$ increases with increasing Ω_0; this is because the underlying strength of the current shocks grows on average as the merging rate (moderately) increases on approaching the critical cosmology (see Lacey & Cole 1993). A similar behaviour is followed by the corresponding dispersion ΔL, see Fig. 10 (right).

Similarly, we derive a correlation with T of the effective size of the X-ray emission. If (following Mohr & Evrard 1997) we define $R_{\rm X}$ in terms of the (high) isophote corresponding to 1.9×10^{-3} count s^{-1} arcmin^{-2} in the *ROSAT* band (consistent with our normalization for L), we find the $\langle R_{\rm X}\rangle$–T correlation shown in Fig. 11. We find $R_{\rm X}\propto T$ in the range of clusters, with a steepening at the group scale and a flattening at large temperatures. A corresponding fitting formula is as follows:

$$
\begin{aligned}
R_{\rm X} &= 1.9 a_R\, T^{0.5+\alpha_R}\,(\rho/\rho_0)^{-1/2},\\
a_R &= 0.6\,\Omega_0^{0.1}\,(1+z)^{-1.5+0.3\,(1-\Omega_0)/(1+z)},\\
\alpha_R &= 0.5\,\Omega_0^{-0.6}\,(1+z)^{0.6}\,{\rm e}^{-0.37\,(T-T_1)\Omega_0^{0.2}/(1+z)^{1.4}},
\end{aligned}
\qquad (16)
$$

where $R_{\rm X}$ is expressed in Mpc and T in keV.

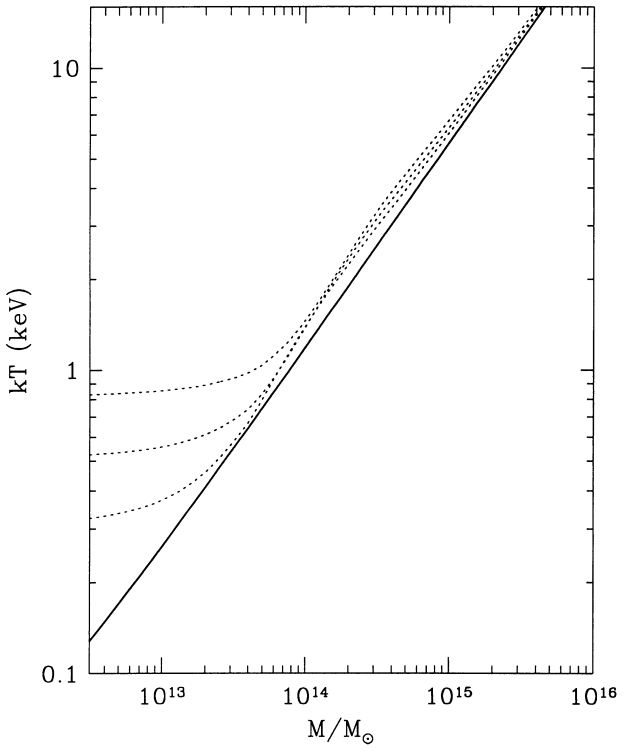

Figure 8. The predicted mass–temperature relation for $T_1 = 0.8$, 0.5, 0.3 and 0 keV, from top to bottom.

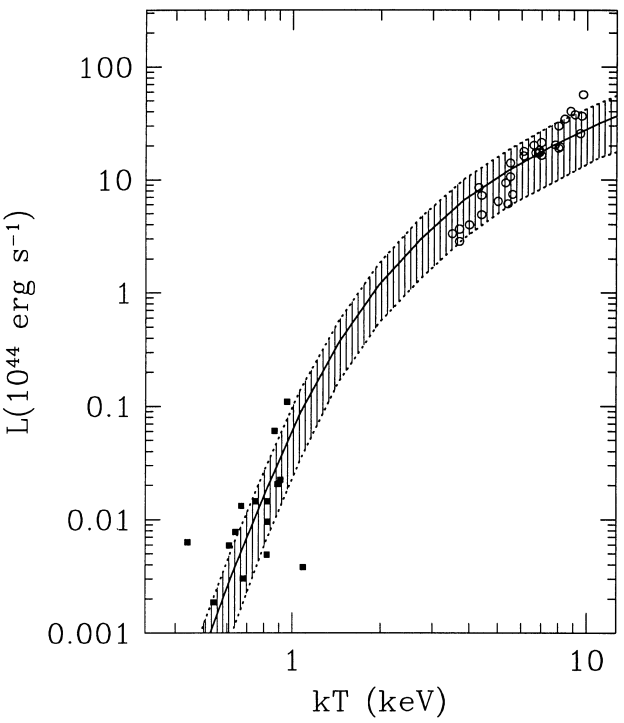

Figure 9. The average L–T correlation with its 2σ dispersion (shaded region) for the PE model with the tilted CDM cosmogony of Fig. 1. The value $H_0 = 50\,{\rm km\,s^{-1}\,Mpc^{-1}}$ is assumed for the Hubble constant. The luminosities are corrected to 0.3 solar metallicity using the standard Raymond–Smith (1977) code. Group data from Ponman et al. (1996, solid squares); cluster data from Markevitch (1998, open circles). Here $T_1 = 0.5$ keV with no dispersion; the effect of the latter is shown by fig. 2 of CMT98.

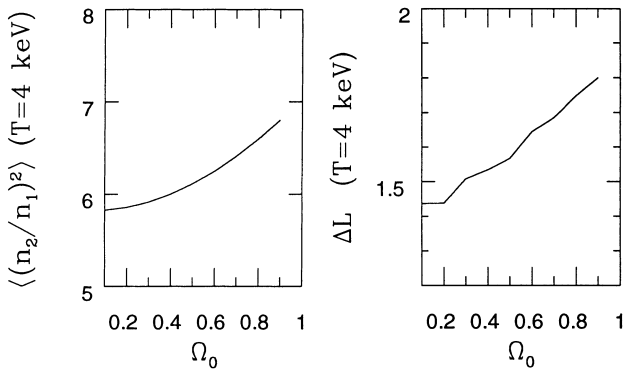

Figure 10. *Left panel*: The dependence of the average luminosity $L \propto \langle(n_2/n_1)^2\rangle$ on Ω_0. *Right panel*: The dependence of the dispersion ΔL on Ω_0. In both panels CDM cosmogonies are assumed, see Liddle et al. (1996).

4 DISCUSSION AND CONCLUSIONS

This paper is based on hierarchical clustering; group and cluster formation is envisaged in terms of DM potential wells evolving hierarchically, and engulfing outer baryons by accretion of smooth gas or by merging with other clumps. In fact, the diffuse baryonic component increases as the deepening wells overcome the external gas energy provided by pre-heating stars or by virialized subclumps. After a merging episode, the ICP in the wells falls back to a new, approximately hydrostatic equilibrium (hence the name 'punctuated equilibria').

We have modelled this complex astrophysics using an *analytic* approach based on the standard hierarchical clustering and comprising three main *steps*: the hydrostatic equilibrium for the ICP is computed for a given boundary condition; the latter is derived from the effects on the ICP of the dynamical evolution of the DM haloes; and the intrinsic stochastic character of such evolution is accounted for on convolving with the statistics of the DM merging histories.

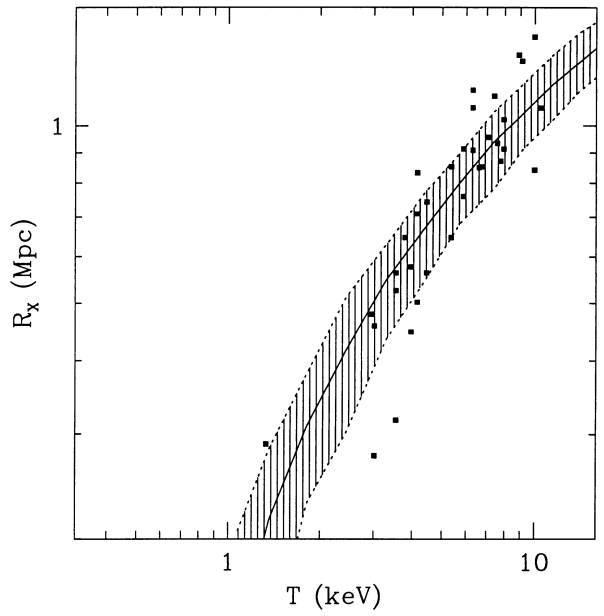

Figure 11. The correlation of the radius R_X (see text) with T (emission-weighted) plotted for $\Omega = 1$. The 2σ dispersion is shown by the shaded region; the cosmological parameters and the perturbation power spectrum are as in Fig. 2. The data are from Mohr & Evrard (1997).

All such aspects are treated in a fashion that is necessarily simplified; however, the resulting model – whose parameters are all internally or physically constrained – proves to be gratifyingly *efficient* in explaining and predicting a variety of observations. We shall discuss such aspects in turn.

As for the ICP *equilibrium*, we note that the condition $R/c_s < t_d$ (sound crossing time shorter than the dynamical time) is weakly satisfied. However, this is enough to ensure ICP equilibrium during the intervals (at least two-thirds of the total time, see Tormen et al. 1997) when the DM haloes themselves are in approximate dynamical equilibrium. In point of fact, ever since Jones & Forman (1984) to the recent Cirimele, Nesci & Trevese (1997), it has been recognized that hydrostatic equilibrium provides for many clusters a fitting description of the averaged profiles of surface brightness in X-rays (except for the central region when cooling flows set in). Even the high-resolution observations provided by *ASCA* (Markevitch 1998) and those being derived from *SAX* data can be accounted for in terms of average profiles. Conspicuous hotspots do occur, but only in a minority of sources, and then in correlation with other signs of ongoing major dynamical events, as discussed next.

This body of evidence supports the case that the gas stays close to hydrostatic equilibrium, or falls back to it after a short transient from the merging event, except for the rare major episodes involving a partner of comparable mass. The limits to the above picture may be defined with the help of aimed hydrodynamical simulations. A quantitative account of how much and how long cluster collisions displace the ICP out of equilibrium can be found, e.g., in the N-body experiment of Roettiger et al. (1998) for the case of a merging event with a mass ratio of 1/2.5. Even for such ratio (already a rare event in the hierarchical clustering picture) the simulation shows that some 2 Gyr after the event hotspots and space variations of the luminosity are reduced to under 20 per cent.

So a sequence of hydrostatic equilibria of the ICP is physically motivated for all merging events except for those involving comparable clumps (a mass ratio larger than $\sim$1/4). However these sum up to less than 10 per cent in the number; in addition, these events yield a shock compression factor $n_2/n_1 \approx 1$ (see equation 9), with an overall contribution to $\langle L\rangle$ less than 10 per cent. This is actually the precision level of our model.

Note that these considerations also support the use of the polytropic relation $T \sim n^{\gamma-1}$. In fact, when equilibrium holds, a macroscopic $\gamma = \mathrm{d}\ln p/\mathrm{d}\ln n$ may always be defined in principle to describe the ICP state; the question concerning whether this is constant on scales $\gtrsim$0.1 Mpc can be probed with observations. In fact, as we discuss later on in this section, observed temperature and surface brightness profiles agree well with those predicted by the polytropic equation of state with $\gamma \approx 1.2 \pm 0.1$.

The hydrostatic equilibrium is described by a first-order differential equation (see Section 2.3) requiring one condition at the *boundary*. Physically, this is provided by the place where a shock converts most of the kinetic and gravitational energy of the inflowing colder gas into thermal energy, as must occur for the accreted ICP to be contained in the well. The boundary condition may be referred to in terms of the stress balance

$$P_2 = P_1 + n_1 m_H v_1^2,$$

one conservation law contributing to equations (8) and (9). If it were somehow possible to shut off the right-hand side completely, the intracluster medium would expand somewhat (the more so the closer is its state to isothermal, and the shallower is the potential at the shock position); the density would decrease everywhere

including the centre and $L \propto n^2$ would quench considerably over a sound crossing time. However, we shall argue next that the dynamic stress acts steadily.

In closer detail, the shock jump conditions are set in terms of T_2/T_1, basically the height of the current potential well (see equation 8) compared with the thermal energy of the infalling gas. The latter is initially due to stellar pre-heating (of nuclear origin); then it is increased to the virial value (of gravitational origin) when the accreted gas is bound in DM subclumps. So the pre-heating sets an effective threshold $kT_1 \sim 0.5$ keV to gas inclusion, which breaks the self-similar correlation $L \propto T^2$ not only in its vicinity but also up to a few keV. In our model, this occurs through the specific dependence of n_2/n_1 on T_2/T_1 at the cluster boundary holding for spherical shocks, strong or weak. This is a fair representation for the conditions prevailing when the cluster growth occurs by nearly isotropic accretion of smooth gas or of many small clumps, as shown by a sequence of spherical hydrodynamical simulations up to the recent one by Takizawa & Mineshige (1998a). This representation looks a rather crude approximation to the aftermaths (lasting up to 2 Gyr) of major merging events, such as those simulated in detail by Roettiger et al. (1998). But in point of fact, our average quantities, their scatter and the profiles agree with the data over the whole range of T as we stress next, while an explanation in point of principle is offered thereafter.

For example, the equilibrium parameter $\beta(T)$ is set by the boundary conditions in terms of shock strengths to values that increase from about 0.5 at the group scale to about 0.9 for rich clusters (see Fig. 2). Correspondingly, the surface brightness profiles in groups – beyond the generally larger observational noise – ought to be flatter than in rich clusters (see Figs 6 and 7). In fact, similar values are obtained from fits to the brightness $\Sigma(r)$ observed in groups and in rich clusters ever since Kriss, Cioffi & Canizares (1983) and Jones & Forman (1984). More recently, a similar trend has been found from spectroscopic measurements of β by Edge & Stewart (1991), and by Girardi et al. (1998). We add that – as another straightforward consequence of the threshold T_1 – our model groups differ from rich clusters also for their lower, average baryonic fraction (see Fig. 3) in accord with the average values inferred by Reichart et al. (1999) from observations, however noisy.

The other parameter of the ICP equilibrium, namely the polytropic index γ, is constrained to the rather narrow range $1 \leq \gamma < 1.3$. The upper bound holds if the ICP thermal energy content is not to exceed its gravitational energy in the DM potential (see Fig. 4); it may be extended to 1.4 only if kinetic energy transfer from residual clumps in DM to ICP contributes more than 20 per cent, the limit set by Kravtsov & Klypin (1998). Values of γ around 1.2 imply the entropy distribution $S(r) \propto \log[T(r)/n^{\gamma-1}(r)]$ to have a neat central minimum, in accord with the notion of dominant entropy deposition by shocks in the outer regions (see David, Jones & Forman 1996; Bower 1997) against the central contribution deposited by supernovae. In fact, specific calculations based on entropy production at the shock show that $\gamma \approx 1.2$ holds with little variations from clusters to groups (Tozzi & Norman, in preparation). Values of $\gamma \approx 1.2 \pm 0.1$ turn out to yield temperature gradients (see Fig. 5) consistent not only with the results from advanced simulations of rich clusters (Bryan & Norman 1998), but also with aimed recent observations by Markevitch et al. (1997) (see also Fusco Femiano & Hughes 1994). Preliminary data from *SAX* (Molendi, private communication) indicate in some cases a somewhat flatter central gradient, but still consistent with the range of γ given above. That such gradients cannot be realistically traced back to imperfect thermalization of the electrons has been argued by Ettori & Fabian (1998) (for a discussion see also Takizawa & Mineshige 1998b). Note that the arguments may be reversed, opening an interesting perspective to gauge the baryon thermal history and its link with the DM dynamics (see Fig. 6); in fact, very steep DM cusps would require larger values of γ to fit the core-like shape of $\Sigma(r)$, but this in turn would produce steep profiles of $T(r)$ and imply additional central inputs of energy and entropy, leading to a strongly bent L–T relation.

As for the *statistical* aspects governing average correlations and their scatter, these are derived from convolution of the boundary conditions over the merging histories. We have already predicted and discussed the L–T correlation in our previous papers (CMT97; CMT98). Here we only note, and illustrate in Fig. 9, the points discussed by Markevitch (1998) and Allen & Fabian (1998): namely, that, once the effect of large cooling flows is removed or accounted for, the average correlation is flattened to a slope around 2.5 and the scatter is reduced down to 13 per cent (1σ), in good agreement with the intrinsic, dynamic scatter from the model.

Here instead we expand on the R_X–T correlation (see Fig. 11). That our model predicts $R_X \propto T$ inside rich clusters, with a steepening at the group temperatures, is due both to the non-self-similar form of the shock strength as a function of T, and to the shape of $\beta(T)$ discussed above. The results agree with the data, whilst all the self-similar computations (including the simulations without pre-heating discussed by Mohr & Evrard 1997) yield $R_X \propto T^{0.5-0.7}$. The dispersion we find from the average over the merging histories also compares well with the existing data.

To understand such overall *effectiveness* of the model one has to consider two features of the hierarchical clustering: (i) the main contributions to the growth of cluster-sized DM haloes is given by the many lesser, closely isotropic events (see Fig. 1), which are described well by the model; and (ii) such events contribute the most to statistics like the $\langle L \rangle$–T correlation, as can be seen on examining the convolutions with the complete merging histories represented by equations (13) and (14). The argument reduced to the bones goes as follows: the average $\langle L \rangle \propto \langle (n_2/n_1)^2 \rangle$ may be expressed by summing the values $(n_2/n_1)^2$ after a merging episode, weighted with the probability Π of a given mass ratio (see bottom panel of Fig. 1), and with the mass increment $\Delta M/M$. Considering a cluster with $M \approx 10^{15}\,M_\odot$, the rare events ($\Pi \approx 0.15$) corresponding to $\Delta M/M \approx 0.5$ yield $(n_2/n_1)^2 \approx 1$; instead, events with $\Delta M/M \lesssim 0.1$ have $\Pi \gtrsim 0.6$ and yield $(n_2/n_1)^2 \gtrsim 6$ [from equation (9) averaged over the merging histories], whose product makes an overwhelming contribution to the average.

In summary, our picture envisages the *combined* effect over the effective time Δt of all shocks that overlap. Barring the lumps too small to overlap and yield an appreciable mass accretion rate, and those too warm and too few to yield relevant compressions, our physical picture is focused on to a nearly *continuous* accretion of intermediate and colder lumps overlapping within a sound crossing time. From these, the ICM feels a nearly steady external pressure with only minor fluctuations. Such pressure exerted at the cluster boundary sets the internal density via the connection between boundary and centre provided by hydrostatic equilibrium, and so determines the steady $\langle L \rangle$, possibly varying on cosmological timescales.

Finally, we stress the *efficiency* of the present analytical approach in making predictions for a wide range of cosmologies/cosmogonies. These are easily spanned in terms of the convolutions (13) and (14) over the merging histories to yield the dependence of the

amplitude, shape and scatter of the predicted correlations L–T, R_X–T on the cosmology as given in Fig. 10 and fitted with equations (15) and (16). Such histories are dominated by those merging events between very *unequal* clumps (with $T_1 \ll T$) which occur *close* to the observation time (Lacey & Cole 1993), as shown in the middle panel of Fig. 1. Though the merging rate does depend on Ω_0, the sum over time of the merging events is weakly dependent on it, and so are the average luminosity and the dispersion (see Fig. 10).

The advances attained by the PE model are as follows. The free parameters (the central density n_c, β and γ) of the previous hydrostatic models are now computed or constrained. The boundary conditions that yield n_c and β are derived from an approximate treatment of the hydrodynamics, and are related to the DM dynamics. The stochastic character of the latter implies variance in the merging histories even at given T, and this is enhanced by the n^2 dependence of the emission to yield the intrinsic scatter expected in L. The resulting, narrowly constrained model predicts temperatures declining outwards, and – in scaling down from rich clusters to groups – smaller β and shallower brightness profiles, decreasing baryonic content on average, and the L–T relation bending down strongly on approaching the pre-heating threshold $kT_1 \sim 0.5$ keV.

Any reasonable spread in such a threshold as discussed by CMT98 implies for groups an increased luminosity dispersion $\Delta L/L > 25$ per cent (2σ) along with a considerable scatter $\Delta f/f \approx \Delta T_1/T_1$ in the baryonic fraction, apart from the larger uncertainties affecting the group observations. We have deliberately chosen to keep the model simple and to implement here neither such spread nor the z dependence of T_1 that is expected for $z \gtrsim 1$, corresponding to the star formation rates at such early z. We plan to expand on such issues while the high-z data are drawing near.

ACKNOWLEDGMENTS

We are indebted to M. De Simone and D. Trevese for communicating their data prior to publication, to F. Governato for discussing with us his high-resolution N-body simulations, and to S. Molendi for several informative discussions concerning the temperature profiles from *SAX*. Thanks are due to our referee C. Lacey for pointing out a number of errors and omissions in the manuscript, and for having stimulated us to clarify the exposition of several important points. Grants from ASI and from MURST are acknowledged.

REFERENCES

Adami C., Mazure A., Katgert P., Biviano A., 1998, A&A, 336, 63
Allen S. M., Fabian A. C., 1998, MNRAS, 297, L57
Balogh M. L., Babul A., Patton D. R., 1998, preprint [astro/ph9809159]
Blanchard A., Valls-Gabaud D., Mamon G., 1992, A&A, 264, 365
Böhringer H., Tanaka Y., Mushotzky R. F., Ikebe Y., Hattori M., 1998, A&A, 334, 789
Bond J. R., Cole S., Efstathiou G., Kaiser N., 1991, ApJ 379, 440
Bower R., 1991, MNRAS, 248, 332
Bower R., 1997, MNRAS, 288, 355
Bryan G. L., Norman M. L., 1998, ApJ, 495, 80
Bunn E. F., White M., 1997, ApJ, 480, 6
Cavaliere A., Fusco Femiano R., 1978, A&A, 70, 677
Cavaliere A., Menci N., Tozzi P., 1997, ApJ, 484, L1 (CMT97)
Cavaliere A., Menci N., Tozzi P., 1998, ApJ, 501, 493 (CMT98)
Cirimele G., Nesci R., Trevese D., 1997, ApJ, 475, 11
Colberg J. M, White S. D. M., Jenkins A., Pearce F. R., 1997, preprint [astro-ph/9711040]
David L. P., Jones C., Forman W., 1995, ApJ, 445, 578
David L. P., Jones C., Forman W. 1996, ApJ, 473, 692
Edge A. C., Stewart G. C., 1991, MNRAS, 252, 428
Ettori S., Fabian A. C., 1998, MNRAS, 293, 33
Fusco Femiano R., Hughes J. P., 1994 ApJ, 429, 545
Gheller C., Pantano O., Moscardini L., 1998, MNRAS, 295, 519
Girardi M., Giuricin G., Mardirossian F., Mezzetti M., Boschin W., 1998, ApJ, 505, 74
Gorski K. M., Ratra B., Stompor R., Sugiyama N., Banday A. J., 1998, ApJS, 114, 1
Henriksen M. J., White R. E. III, 1996, ApJ, 465, 515
Hjorth J., Oukbir J., van Kampen E., 1998, MNRAS, 298, L1
Honda H., Hirayama M., Watanbe M., Yamashita K., Ohashi T., 1997, in Makino F., Mitsuda K., eds, X-ray Imaging and Spectroscopy of Cosmic Hot Plasmas. Univ. Acad. Press, Tokyo, p. 111
Hughes J. P., Gorenstein P., Fabricant D., 1988, ApJ, 239, 82
Jones C., Forman W., 1984 ApJ, 276, 38
Kratsov A. V., Klypin A. A., 1998, preprint
Kriss G., Cioffi D., Canizares C., 1983, ApJ, 272, 439
Lacey C., Cole S., 1993, MNRAS, 262, 627
Lacey C., Cole S., 1994, MNRAS, 271, 676
Liddle A. R., Lyth D. H., Roberts D., Viana P. T. P., 1996, MNRAS, 278, 644
Markevitch M., 1998, ApJ, 504, 27
Markevitch M., Sarazin C. L., Henriksen M. J., 1997, in Makino F., Mitsuda K., eds, X-ray Imaging and Spectroscopy of Cosmic Hot Plasmas. Univ. Acad. Press, Tokyo, p. 91
Markevitch M., Forman W. R., Sarazin C. L., Vikhlinin A. A., 1998, ApJ, 503, 77
Mohr J.J., Evrard A. E., 1997, ApJ, 491, 38
Moore B., Governato F., Quinn T., Stadel J., Lake G., 1997, preprint [astro-ph/970951]
Mushotzky R. F., 1994, in Durret F., Mazure A., Tran Tahn Van J., eds, Clusters of Galaxies. Editions Frontières, Gif-sur-Yvette, p. 177
Mushotzky R. F., Scharf C. A., 1997, ApJ, 482, L13
Navarro J. F., Frenk C. S., White S. D. M., 1997, ApJ, 490, 493
Peebles P. J. E., 1993, Principles of Physical Cosmology. Princeton Univ. Press, Princeton
Perrenod S. C., 1980, ApJ, 236, 373
Ponman T. J., Bourner P. D. J., Ebeling H., Böhringer H., 1996, MNRAS, 283, 690
Press W. H., Schechter P., 1974, ApJ, 187, 425
Raymond J. C., Smith B. W., 1977, ApJS, 35, 419
Reichart D. E., Nichol R. C., Castander F. J., Burke D. J., Romer A. K., Holden B. P., Collins C. A., Ulmer M. P., 1999, ApJ, 518, 521
Renzini A., 1997, ApJ, 488, 35
Roettiger K., Stone J. M., Mushotzky R. F., 1998, ApJ, 493, 62
Sarazin C. L., 1988, X-ray Emission from Clusters of Galaxies. Cambridge Univ. Press, Cambridge
Schindler S., Müller E., 1993, A&A, 272, 137
Suginohara T., Ostriker J. P., 1998, ApJ, 507, 16
Takizawa M., Mineshige S., 1998a, ApJ, 499, 82
Takizawa M., Mineshige S., 1998b, preprint [astro-ph/9807003]
Tormen G., Bouchet F. R., White S. D. M., 1997, MNRAS, 284, 865
Tsuru T., Koyama K., Hughes J., Arimoto N., Kii T., Hattori M., 1996, in Yamashita K., Watanabe T., eds, UV and X-Ray Spectroscopy of Astrophysical and Laboratory Plasmas. Universal Academy Press, Tokyo, p. 375
White M., Viana P. T. P., Liddle A. R., Scott D., 1996, MNRAS, 283, 107
White S. D. M., Fabian A. C., 1995, MNRAS, 273, 72
White S. D. M., Rees M., 1978, MNRAS, 183, 341
White S. D. M., Navarro J. F., Frenk C. S., Evrard A. E., 1993, Nat, 366, 429

This paper has been typeset from a TEX/LATEX file prepared by the author.